

HYDRODYNAMIC MODELING OF NEW RIVER INLET, NORTH CAROLINA USING NearCoM-TVD

Jia-Lin Chen¹, Tian-Jian Hsu¹, Fengyan Shi¹, Britt Raubenheimer², and Steve Elgar²

The goal of this study is to investigate the role of wave-current interaction in tidal inlet hydrodynamics. A quasi-3D nearshore community model, NearCoM-TVD, is used to simulate circulation and waves at New River Inlet, NC, USA. Model skill for waves and circulation is evaluated at about 30 locations throughout the inlet, including a recently dredged navigation channel, a shallower channel, a flood tidal delta, and ebb tidal deltas, for a range of flow conditions in May 2012. Model skills for flow velocity and wave height are high in the channels. The numerical model also captures the sharp transition between wave-dominated and tide-dominated flows near the ebb tidal deltas. Model results demonstrate that wave intensity plays an important role in circulation (vortex) generation near inlet entrances.

Keywords: New River; NearCoM-TVD; wave-current interaction; tidal inlet;

INTRODUCTION

Inlet hydrodynamics is critical to many coastal engineering applications. Due to complex interactions between tidal currents, waves, and bathymetry, highly (spatially and temporally) variable flows can be generated in an inlet system. Understanding these nonlinear processes and resulting morphological evolution can be a challenge, and a validated numerical model can be a useful tool for these purposes (Elias et al. 2006; Bertin et al. 2009; Malhadas et al. 2009; and Keshtpoor et al. 2014).

Many prior studies have focused on the hydrodynamics of tidal inlets under the interaction between mean (tidal) currents and the bathymetry (de Swart and Zimmerman 2009). In the absence of waves, the leading order terms in the momentum balance are the horizontal pressure gradient and the bottom shear stress (Hench and Luettich 2003). However, waves can dominate inlet processes via current-induced refraction and Doppler shifts, steepening of waves propagating into opposing currents, and enhanced roughness experienced by currents owing to the wave bottom boundary layer (Wolf and Prandle, 1999). For example, recent studies at Katama Inlet, MA during Hurricane Irene (Orescanin et al., 2014) and at New River Inlet during Tropical Storm Alberto (Wargula et al., 2014) show the gradient of radiation stress induced by breaking waves can enhance landward-directed flows.

In this study, a numerical investigation on wave-current-bathymetry interactions at New River Inlet, NC, is carried out in conjunction with a multi-institutional field experimental campaign (MacMahan et al., 2014; Wargula et al., 2014; Rogowski et al., 2014). A curvilinear nearshore circulation model, SHORECIRC (Svendsen et al. 2004), has been adapted into a hybrid finite-difference/finite-volume, TVD-type scheme (Toro, 2009) and coupled with the wave-spectrum model SWAN (Booij et al. 1999). The quasi-3D circulation model includes the effects of waves on the vertical structure of the currents based on theory (Putrevu & Svendsen, 1999). The numerical model is fully parallelized with MPI and is suitable for long-term (months), large-scale [$O(10\sim 100)$ km] simulations. Conventional finite-difference schemes often produce unphysical oscillations when modeling coastal processes with abrupt changes or discontinuities, such as tidal bores, breaker zones, and moving shorelines. In contrast, the TVD-type finite volume scheme allows for robust treatment of discontinuities through the shock capturing mechanism. To demonstrate the capability of the newly developed model, NearCoM-TVD was verified and validated with several coastal applications (Chen et al. 2014). In particular, the modeled flow velocity through an idealized tidal inlet was compared with an analytical solution (Keulegan, 1967). Furthermore, to evaluate the model's capability for applications with wave-current interaction, the modeled wave heights and current velocities over a shoals and rip channel system were compared with the measured data during a rip-current field experiment (MacMahan et al., 2010). Here, NearCoM-TVD is applied to study hydrodynamics and sediment transport at New River Inlet, NC under the interaction of tides and waves. A comprehensive model skill assessment in different sections of the inlet system is presented for both significant wave height and circulation velocities. The numerical model is then used to study the flow patterns resulting from waves from different directions.

MODEL EQUATIONS

NearCoM-TVD (Shi et al. 2013; Chen et al. 2014) couples the spectral wave model SWAN (Booij et al. 1999) and a quasi-3D nearshore circulation model SHORECIRC (Svendsen et al. 2004). SHORECIRC is a two-dimensional horizontal (2DH) model that incorporates the mixing effect

¹ Civil and Environmental Engineering, University of Delaware, Newark, DE, 19702, USA

² Woods Hole Oceanographic Institution, MA, 02543, USA

induced by the vertical variation of wave-induced horizontal circulation. Similar to most of the river inlet systems in the southern part of North Carolina, fresh water discharge from New River is relatively low (Pilkey et al. 1998). For this well-mixed coastal environment with negligible baroclinic gradients, the present quasi-3D model is shown to produce results similar to those of fully 3D circulation models (Haas and Warner, 2009).

The instantaneous horizontal velocity u_α^{ins} in Cartesian coordinates x_1, x_2 is split into (Putrevu and Svendsen, 1999)

$$u_\alpha^{ins} = u'_\alpha + u_{w\alpha} + u_\alpha + u_{1\alpha} \quad (1)$$

where $\alpha = 1$ is the east-westward direction and $\alpha = 2$ is the north-southward direction. u'_α , $u_{w\alpha}$, u_α , and $u_{1\alpha}$ represent the turbulent velocity fluctuation, the wave velocity, the depth-averaged short-wave-averaged velocity, and the vertical variation of the short-wave-averaged velocity, respectively. The depth-averaged and short-wave-averaged velocity u_α is defined by ‘Lagrangian averaging’ as

$$u_\alpha = \frac{1}{H} \overline{\int_{-h}^{\zeta} u_\alpha^{ins} dz} \quad (2)$$

where ζ is the instantaneous surface elevation and the total water depth $H = \eta + h$, in which h is the still water level and η represents the wave-averaged surface elevation.

A coordinate transformation is performed between the Cartesian coordinates x_α and the generalized curvilinear coordinates ξ^α , and thus the contravariant components of the velocity vector can be expressed by

$$u^\alpha = u_\beta \frac{\partial \xi^\alpha}{\partial x_\beta} \quad (3)$$

where the superscript $()^\alpha$ represents the contravariant component of a vector, and subscript $()_\alpha$ is the Cartesian component of a vector. To use the TVD numerical scheme, a conservative form of the equations is derived (Chen et al. 2014) in generalized curvilinear coordinates, given by

$$\frac{\partial \eta}{\partial t} + \frac{1}{J} \frac{\partial J P^\alpha}{\partial \xi^\alpha} = 0 \quad (4)$$

$$\frac{\partial H u_\alpha}{\partial t} + \frac{1}{J} \frac{\partial}{\partial \xi^\beta} \left[J P^\beta u_\alpha + \frac{1}{2} g (\eta^2 + 2\eta h) J \frac{\partial \xi^\alpha}{\partial x^\beta} \right] + f_\alpha - g \eta \frac{1}{J} \frac{\partial}{\partial \xi^\beta} \left(h J \frac{\partial \xi^\alpha}{\partial x^\beta} \right) + \frac{1}{\rho J} \frac{\partial}{\partial \xi^\gamma} \left(S_{\alpha\beta} J \frac{\partial \xi^\gamma}{\partial x^\beta} \right) + \frac{1}{J} \frac{\partial}{\partial \xi^\gamma} \left(\tau_{\alpha\beta} J \frac{\partial \xi^\gamma}{\partial x^\beta} \right) + \frac{\tau_\alpha^b}{\rho} - \frac{\tau_\alpha^s}{\rho} + ROT = 0 \quad (5)$$

where J is the Jacobian determinant. $P^\alpha = H u^\alpha$ denotes the contravariant component of volume flux. In equation (5), all vector forcing terms are in Cartesian coordinates so there is no need to make a transformation for the second-order tensor. f_α represents the Cartesian components of the Coriolis force, i.e., $-f_c H u_2$, $-f_c H u_1$, where f_c is the Coriolis coefficient, u_2 is the south-northward velocity, and u_1 is the east-westward velocity. $S_{\alpha\beta}$ is the Cartesian component of radiation stress (Longuet-Higgins, 1962, 1964), τ_α^b is the Cartesian component of bottom stress, and τ_α^s is wind stress (Van Dorn, 1953), and ROT represents the remaining terms associated with diffusion, atmospheric pressure, and 3D dispersion (Shi et al. 2003).

To lowest order, the equation governing the vertical structure of horizontal velocity is

$$\frac{\partial u_{1\alpha}^{(0)}}{\partial t} - \frac{\partial}{\partial z} \left(\nu_t \frac{\partial u_{1\alpha}^{(0)}}{\partial z} \right) = F_\alpha \quad (6)$$

where ν_t is the eddy viscosity and F_α is a general form of the local forcing (see equation (31) in Putrevu and Svendsen, (1999) for details). The solution of depth variant current velocity $u_{1\alpha}$ is the same as that discussed previously (Shi et al. 2003). The bottom current velocity u_α^b can be evaluated using u_α and $u_{1\alpha}$ at $z = -h$

$$u_{\alpha}^b = u_{\alpha} + u_{1\alpha} (z = -h) \quad (7)$$

The bottom friction is enhanced by wave-current interactions owing to bottom boundary layer processes, and is not simply a linear sum of the wave-induced and current-induced friction. Many theories and models have been proposed to describe the nonlinear behavior of wave-current interaction (e.g., Grant and Madsen, 1979). For the purpose of computational efficiency, a data-based method that had been used for fitting to theoretical models is applied (Soulsby et al., 1993). The bottom friction under the interaction of currents and waves can be estimated by

$$\tau_{\alpha}^b = y (\tau_{\alpha}^c + \tau_{\alpha}^w) \quad (8)$$

where τ_{α}^c is the current-only bottom stress, τ_{α}^w is the wave-only bottom stress, and

$$y = x [1 + bx^p(1 - x)^q] \quad (9)$$

with

$$x = \tau_{\alpha}^c / (\tau_{\alpha}^c + \tau_{\alpha}^w) \quad (10)$$

and

$$b = (b_1 + b_2 |\cos \phi|^{8.8}) + (b_3 - b_4 |\cos \phi|^{8.8}) \log_{10} \frac{f_w}{C_D} \quad (11)$$

where f_w is the friction factor used to compute τ_{α}^w , and C_D is the friction factor used to compute τ_{α}^c . As suggested previously (Soulsby 1997), f_w is calculated from an explicit formula (Swart 1974), and C_D can be obtained from the logarithmic velocity profile with a given roughness length z_o , here assumed to be $z_o = 0.001$ m. The fitting coefficients in (11) are b_1 , b_2 , b_3 , and b_4 and the coefficients of the analogous expressions for p and q can be found in Soulsby (1997).

Model Setup

A multi-institutional field study of inlet dynamics was conducted at New River Inlet, NC in May 2012 (MacMahan et al., 2014; Wargula et al., 2014; Rogowski et al., 2014). New River Inlet is located in the southeast of North Carolina. The inlet entrance (Figure 1a) includes a newly dredged channel (3<depth<10m), a shallower channel (depth < 3m), a flood tidal delta, and ebb tidal deltas on both sides and in the middle of the mouth. The bathymetry surveyed on 1 May 2012 covering the inlet and ebb tidal deltas is integrated with earlier, larger-scale surveys to provide the bathymetry used in the present numerical investigation. The model domain includes the inlet channels, the surf zone, the continental shelf, and the large lagoon area behind the inlet. The tidal constituents provided by the ADCIRC (Luettich et al. 1992) database are applied to the western, southern, and eastern open boundaries of the circulation model SHORECIRC. The ADCIRC database provides tidal phases and amplitudes of the M2, S2, N2, K2, O1, and K1 tidal constituents. The boundaries adjacent to the lagoons and the backbay area are closed. The significant wave height and peak period observed at NOAA station 41036 (25 m depth) are applied to the southern boundary of the spectral wave model SWAN. The mean wave direction observed by NOAA station 41109 (13 m depth) is used instead of that observed by NOAA station 41036 for which only 67% of data is available. Observed wind speed and direction measured near the inlet mouth also are used in the circulation and spectral wave models. The Coriolis parameter is calculated using the latitude of New River Inlet 34.10N.

Model Validation

The model results are compared with data from an array of colocated pressure gauges and current meters deployed along a newly dredged channel, a shallower channel, and ebb tidal deltas on both sides and in the middle of the river mouth (Wargula et al., 2014) (see Figure 1a for locations). To compare with modeled results, the current velocities measured with current profilers (at sensors S0, S1, S2, S3, S4, S5, S6, S7, S8, and S9) are depth-averaged. For the rest of the sensors, current velocities are measured at approximately 90 cm above the seafloor (not accounting for the erosion and accretion of the seafloor during the 1-month study).

The accuracy of the model predictions is assessed using the Wilmott skill (Wilmott, 1981),

$$\chi = 1 - \frac{\sum_{i=1}^N |X_{\text{mod}} - X_{\text{obs}}|^2}{\sum_{i=1}^N |X_{\text{mod}} - \bar{X}_{\text{obs}}| + |X_{\text{obs}} - \bar{X}_{\text{obs}}|^2} \quad (12)$$

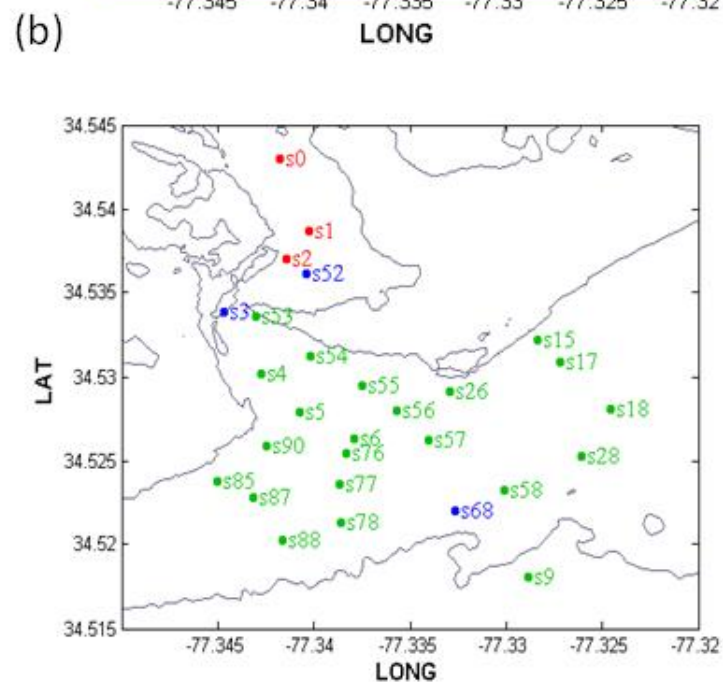
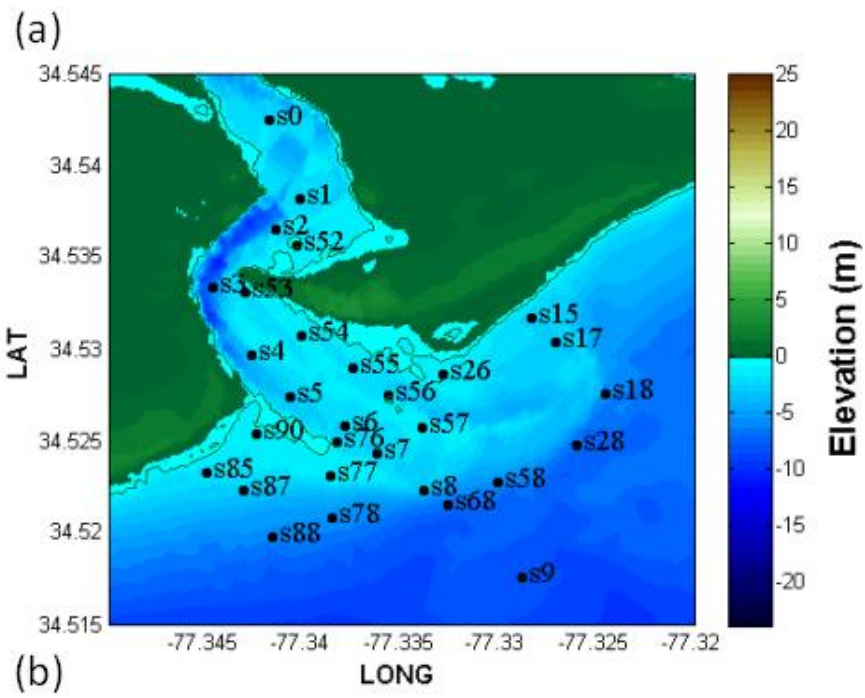
where N represents the sample size, X is the variable being compared, \bar{X} is the sample mean, and the subscripts ()_{mod} and ()_{obs} represent the model result and observed data, respectively. To facilitate the discussion here, model skill greater than 0.6 is categorized as good (or very good when χ at a few locations exceeds 0.8), while model skill below 0.3 is considered poor. Fair model skill is in between 0.3 and 0.6 ($0.3 < \chi < 0.6$).

In the following discussion, the model performance is assessed primarily based on the model skill χ . The RMS magnitude sometimes is referred to when the magnitude of the observed value is small. To understand the magnitude and distribution of the wave and circulation fields at different locations of the inlet, the RMS values for measured wave height or velocities are calculated by

$$H_{\text{rms}} = \sqrt{\frac{1}{N} (\sum_{i=1}^N H_{\text{obs}}^2)} \quad (13)$$

The model skill at predicting wave heights is high for sensors located seaward of the surf zone (for example, see sensor S88 ($\chi=0.77$), S78 (0.76), S18 (0.91), S58 (0.70), S28 (0.71), and S68 (0.59) (Figure 1)). Due to the effect of the ebb tidal jet, which will be discussed in the next section, the model skill is slightly lower at sensor S68 ($0.3 < \chi < 0.6$, blue, Figure 1b). The model also has good skill for sensors located in the surf zone of the south ebb tidal delta (for example, see S87 ($\chi=0.87$), S85 (0.70), S77 (0.77), S76 (0.82), and S90 (0.84) (Figure 1)). Sensors S77 and S85 have slightly lower skill than S87, S76, and S90 because the model predicts less tidal modulation than is observed due to the complexity of wave-current interaction in the breaking zone. In the newly dredged deeper channel, model skill is good at sensors S6 ($\chi=0.75$), S5 (0.87), S4 (0.73), and S3 (0.60). Model skill is low in the region where the main channel makes a 90-degree turn (for example, see S2 (0.16), S1 (0.26), and S0 (0.14)). Model skill is higher in the outer channel than in the inner channel where wave amplitude is already small (observed RMS height below 0.05 m at S2, S1, and S0). Model skill is reasonably good in the shallower channel, for example, see S57 ($\chi=0.76$), S56 (0.82), S55 (0.87), and S54 (0.82). The lower skill values obtained at S52 (0.41), and S53 (0.65) are possibly owing to uncertainties in local bathymetry. The bathymetry around the flood tidal delta (the shallower area between S52 and S53) is not provided by the survey on the 1 May, 2012. Generally, the model predicts the observed wave heights skillfully.

The modeled east-westward velocity u and north-southward velocity v are compared with the measured velocities. In the newly dredged (deeper) channel, the overall model skill for east-westward velocity and north-southward velocity (shown in green in Figure 1c and d) are reasonably good, for example, see S76 (model skill of east-westward velocity/north-southward velocity: $\chi=0.85/0.88$), S6 (0.92/0.91), S5 (0.96/0.95), S4 (0.80/0.85), S2 (0.83/0.86), S1 (0.85/0.84), and S0 (0.89/0.93). Model skill is lower at sensor S3 (0.48/0.92) possibly due to uncertainties in local bathymetry.



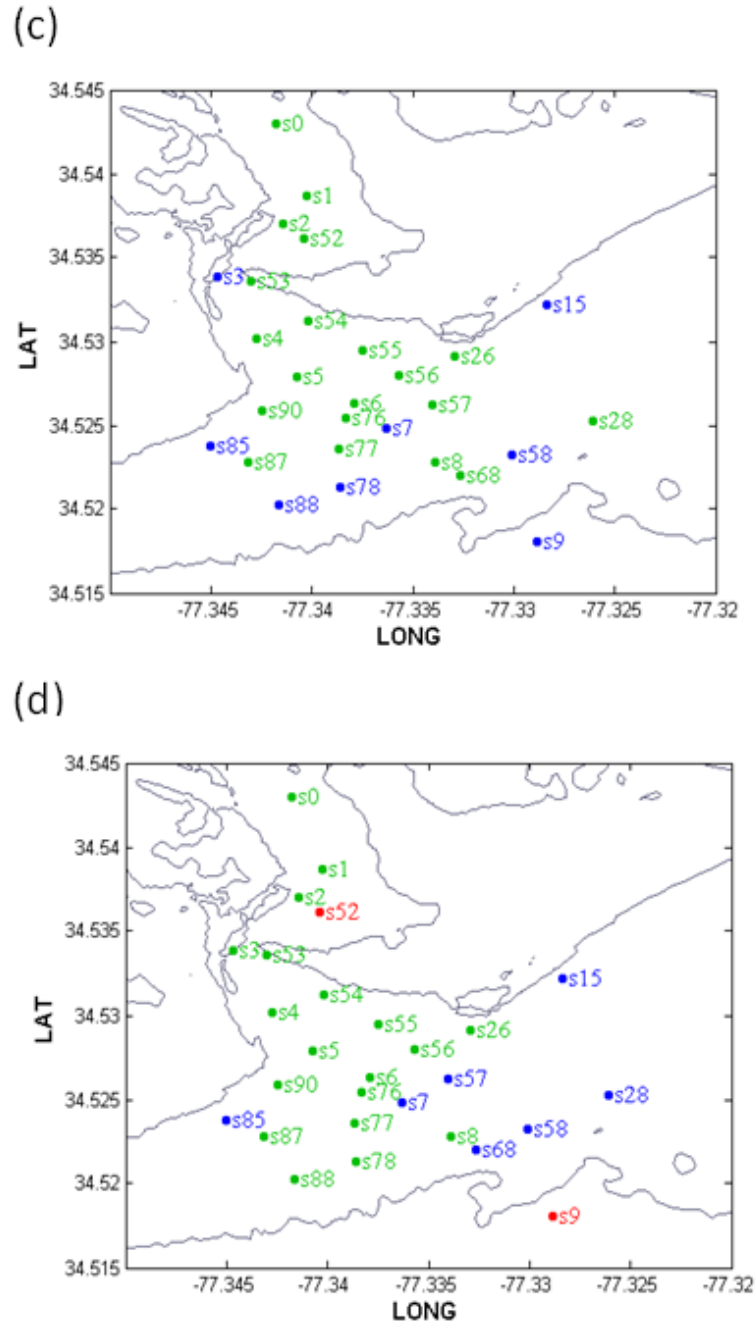


Figure 1 (a): locations of colocated pressure gauges and current meters and bathymetry (color contours), and (b) model performance of predicted significant wave heights, (c) east-westward velocities, and (d) north-southward velocities. The black solid curves are the 0 (shoreline) and 8 m depth contours. The sensor numbers are shown in green if model skill $\chi > 0.6$, in blue if $0.6 > \chi > 0.3$, and in red if $\chi < 0.3$.

The numerical model predicts the phase and the magnitude of the velocity observed through the channel. In the shallower channel, model skill is good at sensor S26 (0.90/0.75), S54 (0.92/0.87), S55 (0.95/0.93), and S56 (0.93/0.93), but is lower at S57 (0.69/0.50) due to the interaction of waves with the tidal jet (Figure 1d). The numerical model simulates accurately the observed velocity magnitude and phase at the mouth of the inlet in the shallower channel (S56, Figure 2). Similar to the wave prediction, model skill values are low near the bend in the inlet channel at S52 (0.68/0.23) and S53 (0.78/0.69) (Figure 1d), possibly owing to the poorly resolved flood tidal delta.

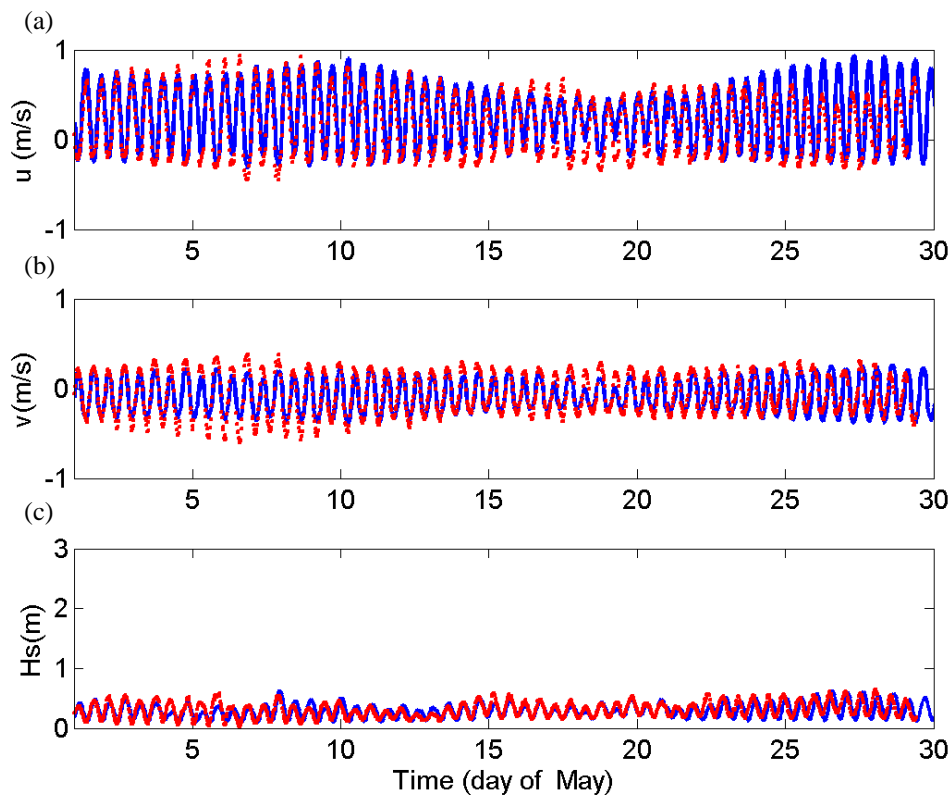


Figure 2: Modeled (blue curves) and measured (red dots) (a) east-west (u) velocity, (b) north-south (v) velocity, and (c) significant wave height (H_s) at sensor 56 in the channel (Figure 1a) versus time.

As an example of moderate model skill, modeled velocities and waves are compared with the measured values at *S77* (0.67/0.86) (Figure 3). Consistent with wave predictions, model skill for *S77*, located on the south ebb tidal delta near the inlet entrance, is lower due to the complexity of wave-current interaction in the breaking zone. Model skill also is lower near the north side of the entrance near sensor *S15* (0.39/0.47) where the current magnitude is low (RMS velocity = 0.16/0.10 m/s). Model skill also is low at *S88* (0.58/0.64), *S78* (0.45/0.66), *S68* (0.64/0.42), *S58* (0.55/0.43), and *S28* (0.64/0.50) where current magnitudes are low, with RMS velocities around 0.05 m/s. It is more difficult to predict currents and waves at the two sides of the inlet entrance, for example, see *S85* (0.49/0.6) and *S15* (0.39/0.47). The model has better skill at sensor *S26* (0.9/0.75), possibly because the model predicts the observed eddy structures. The simulated eddy structures on the two sides of inlet entrance will be discussed in the next section. Model skill varies spatially depending on the complexity of the interactions between currents, bathymetry, and waves. Overall, the predicted flow velocities and significant wave heights agree reasonably well with the measured data.

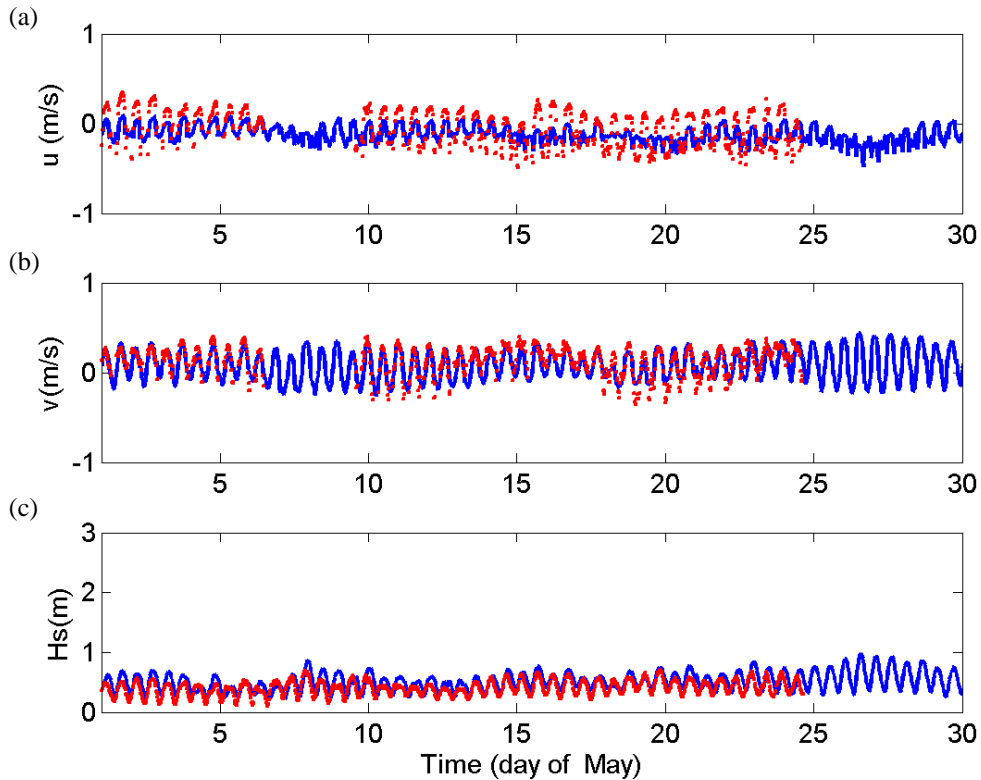


Figure 3: Modeled (blue curves) and measured (red dots) (a) east-west (u) velocity, (b) north-south (v) velocity, and (c) significant wave height (H_s) at sensor 77 on the outer edge of the ebb tidal delta (Figure 1a) versus time.

FLOW PATTERNS

The snapshots of model results on May 12 at maximum flood tide (01:00 am EDT) and maximum ebb tide (08:00 am EDT) near the inlet illustrate the flow patterns (Figure 4). May 12 is a period of spring tide (tidal amplitude 0.7 m) and mild wave conditions (offshore significant wave height is slightly below 1 m). During maximum flood (Figure 4a), flow is funneled into the inlet due to the water level difference between the inlet and the open sea. Peak flow velocities in the deeper (southwestern) channel exceed 1.0 m/s in magnitude, while in the southwestern ebb tidal delta, peak flow intensity is around 0.4 m/s. During the maximum ebb (Figure 4b), the instantaneous flow field shows the characteristics of an ebb tidal jet, with the strongest flow intensity (>1.5 m/s) in the channels. However, flows on the southwestern and northeastern ebb tidal deltas also are large. Near the inlet entrance where the deeper and the shallower channels are separated by the central ebb tidal delta, the tidal jet splits into two. The jet at the southwestern side of the inlet is stronger and wider than the jet in the northeast. During maximum ebb flow, this main jet can penetrate all the way through the surf zone to 8 m water depth or more. Slightly west of the jet, the ebb flow intensity is attenuated sharply near the outer edge of the southwestern ebb tidal delta. The weaker ebb tidal jet originating from the shallower channel is diverted farther northeastward in the alongshore direction. A weak circulation pattern is observed just off the northeastern shore (indicated by the box in Figure 4b), possibly due to the interactions between currents and waves.

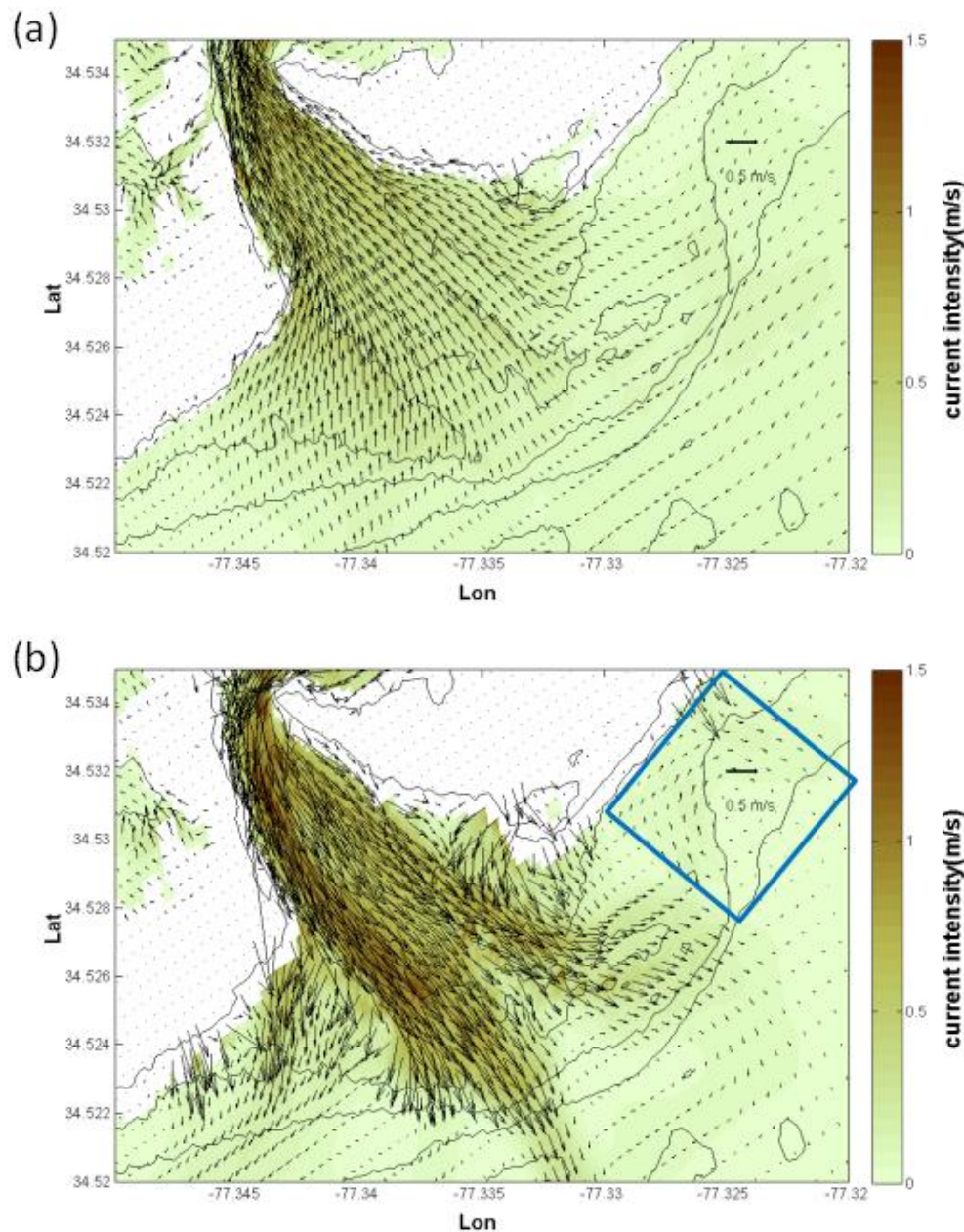


Figure 4: Modeled instantaneous flow field (vectors indicate direction and color contours indicate current intensity) during (a) maximum flood and (b) maximum ebb on May 12. The solid curves are bathymetric contours (0, 2, 4, 6, and 8 m depth relative to NAVD 88).

The validated numerical model can be a useful tool to understand nearshore circulation patterns in a tidal inlet and to illustrate the role of wave-current interaction. To investigate the effect of waves, a numerical simulation of a spring-tide large-wave condition using the M2 tidal amplitude of May 12 and offshore waves (significant wave height 3m) from the southeast (similar to those observed by NOAA station 41036 at 14:50 pm EDT on May 26th during the tropical storm Alberto) was performed. Instantaneous flow fields were simulated for maximum flood and maximum ebb (Figure 5a and b). Under a mild wave condition, the clock-wise circulation pattern in the northeastern shore is weak during maximum ebb flow (see the box in Figure 4b). However, when waves become more energetic, this circulation pattern becomes pronounced throughout the entire tidal cycle (Figure 5a and b). During the maximum ebb flow, the direction of the ebb tidal jet in the shallower (northeastern) channel is tilted northeastward, and feeds into the clockwise northeastern circulation. Hence, the simulations suggest

circulation pattern in the northeastern shore is mainly caused by waves. In contrast, the flow through the deeper (southwestern) channel is relatively unaffected by the waves. To understand the effects of incident wave angle, the modeled instantaneous flow fields for waves from the southeast (Figure 5a,b) are compared with the flow fields for waves from the southwest (Figure 5c,d). (Note that energetic waves incident from the southwest were observed during the North American storm complex on December 25–28, 2012, which produced both a tornado outbreak and a blizzard across the southern and eastern United States). During the maximum flood, more intense flood velocities are predicted in both channels and on the northeastern shoals when waves are incident from the southwest. Strong alongshore currents also can be observed near the northeastern and southwestern shores. During the maximum ebb flow, the direction of the ebb tidal jet also is tilted northeastward in the deeper (southwestern) channel adjacent to a more pronounced counter-clockwise circulation pattern in the southeastern shoals (Figure 5d). These simulations suggest that wave direction plays a major role in the flow pattern near the ebb tidal deltas and adjacent shores.

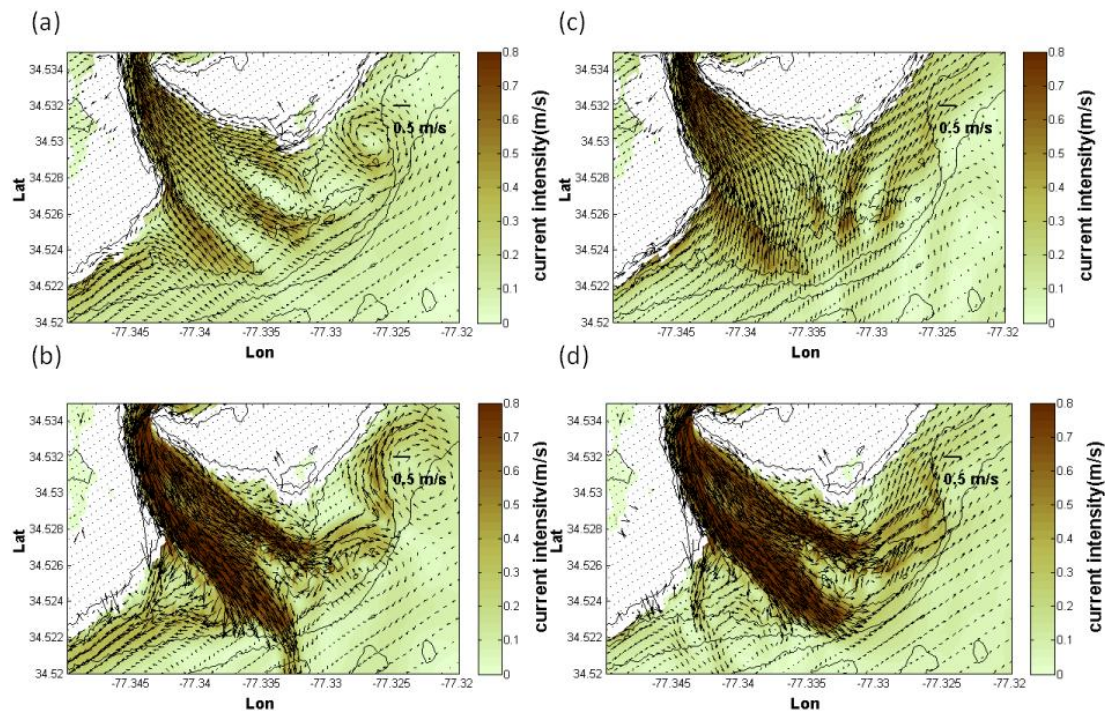


Figure 5: The instantaneous flow field (vectors indicate direction and color contours indicate current intensity) during (a) and (c) maximum flood and (b) and (d) maximum ebb for a spring-tide condition with stormy waves incident from the southeast [(a) and (b)] and from the southwest [(c) and (d)]. The solid curves indicate the contours of 0, 2, 4, 6, and 8 m depth.

CONCLUSION

Hydrodynamics in New River Inlet, NC were studied using NearCoM-TVD (Shi et al. 2013; Chen et al. 2014), which consists of a new version of the quasi-3D nearshore circulation model SHORECIRC (Svendsen et al. 2004) coupled with the spectral wave model SWAN (Booij et al. 1999). The numerical model is validated with data from 30 colocated wave gauges and current meters during a one-month long field experiment encompassing a range of tidal and wave conditions. The numerical model reproduces the observed flow patterns and magnitudes throughout the nearshore and the inlet, including along two channels and on the ebb tidal deltas. Specifically, model skill is high in the channels inland to the region where the main channel makes a 90-degree turn. The validated model is used to provide insights into the complex flow patterns of tidal inlet hydrodynamics. The simulated instantaneous flow field during spring tides and energetic waves demonstrates that waves play important roles in directing tidal flow near the mouth and generating circulation (vortex) patterns around the ebb tidal deltas and adjacent shores.

ACKNOWLEDGMENTS

Funding for this study was provided by the Office of Naval Research (N00014-13-1-0120) and (N00014-13-10106) and the Assistant Secretary of Defense R&E. The authors thank Jesse McNinch of

the U.S. Army Corps of Engineers (USACE) for sharing the bathymetry data of New River Inlet, NC, Ad Reiniers and Jamie MacMahan for sharing the updated bathymetry in the backbay, Jim Thomson for sharing the wind measurements, and the PVLAB field crew and staff of the USACE for deploying, maintaining, and recovering the field instrumentation.

REFERENCES

- Bertin, X., Fortunato, A. B., and Oliveira, A. 2009. A modeling-based analysis of processes driving wave-dominated inlets, *Cont. Shelf Res.*, 29, 819 – 834.
- Booij, N., Ris R.C., and Holthuijsen, L.H. 1999. A third-generation wave model for coastal regions, *J. Geophys. Res.*, 104 C4 , 7649-7666.
- Chen, J.-L., Shi, F., Hsu, T.-J. and Kirby, J.T. 2014. NEARCOM-TVD - A quasi-3D nearshore circulation and sediment transport model, *Coastal Eng.*, 91, 200-212.
- de Swart H. E., and Zimmerman, J.T.F. 2009. Morphodynamics of Tidal Inlet Systems, *Annu. Rev. Fluid Mech.*, 41:203–29.
- Elias, E. P. L., Cleveringa, J., Buijsman, M. C, Roelvink, J. A., and Stive, M. J. F. 2006. Field and model data analysis of sand transport patterns in Texel tidal inlet, *Coastal Eng.*, 53, 505-529.
- Grant, W. D., and Madsen. O. S. 1979. Combined wave and current interaction with a rough bottom, *J. Geophys. Res.*, 89, 1797–1808.
- Haas, K. A., and Warner, J. C. 2009. Comparing a quasi-3D to a full 3D nearshore circulation model: SHORECIRC and ROMS, *Ocean Modell.*, 26 1–2 , 91–103.
- Hench, J.L., Luettich, R.A.Jr. 2003. Transient tidal circulation and momentum balances at a shallow inlet, *J. Phys. Oceanog.*, 33:913–32.
- Keshtpoor, M., Puleo, J., Shi, F., and DiCosmo, N. 2014. Numerical Simulation of Nearshore Hydrodynamics and Sediment Transport Downdrift of a Tidal Inlet, *J. Waterway, Port, Coastal, Ocean Eng.*, 10.1061/ ASCE WW.1943-5460.0000273 , 04014035.
- Keulegan, G.H. 1967. Tidal Flow in Entrances: Water Level Fluctuations of Basins in Communication with the Seas, *Committee on Tidal Hydraulics Technical Bulletin No.14*, U.S. Army Engineers Waterways Experiment Station, Vicksburg, MS.
- Kumar, N., Voulgaris, G., Warner, J.C. 2011. Implementation and modification of a three-dimensional radiation stress formulation for surf zone and rip-current applications, *Coastal Eng.*, 58, 1097-1117.
- Longuet-Higgins, M. S., and Stewart R. W. 1962. Radiation stress and mass transport in gravity waves, with application to ‘surf beats’, *J. Fluid Mech.* 13 4 , 481–504
- Longuet-Higgins, M. S., and Stewart R. W. 1964. Radiation stresses in water waves; a physical discussion, with applications, *Deep-Sea Research*, pp. 529 to 562.
- Luettich, R.A. and Westerink, J.J. 1991. A solution for the vertical variation of stress, rather than velocity, in a three-dimensional circulation model, *International Journal for Numerical Methods in Fluids*, 12:911-928.
- MacMahan, J., Brown J., Thornton. E., Reniers, A., Stanton, T., Henriquez, M., Gallagher, E., Morrison, J., Austin, M.J., Scott, T.M., Senechal, N. 2010. Mean Lagrangian flow behavior on an open coast rip channeled beach: A new perspective, *Mar. Geol.*, 268, 1-15.
- MacMahan, J., van de Kreeke, J., Reniers, A., Elgar, S., Raubenheimer, B., Thornton, E., Weltmer, M., Rynne, P., and Brown, J. 2014. Fortnightly Tides and Subtidal Motions in a Choked Inlet., *Estuarine, Estuarine Coastal Shelf Sci.* doi:10.1016/j.ecss.2014.03.025. [in press].
- Malhadas, M. S., Leitao, P. C., Silva, A., and Neves, R. 2009. Effect of coastal waves on sea level in Óbidos Lagoon, Portugal, *Cont. Shelf Res.*, 19 9 , 1240 – 1250.
- Olabarrieta, M., Warner, J. C., and Kumar, N. 2011. Wave-current interaction in Willapa Bay, *J. Geophys. Res.*, VOL. 116, C12014.
- Orescanin, M., Raubenheimer, B., and Elgar, S. 2014. Observations of wave effects on inlet circulation, *Cont. Shelf Res.*, 82 2014 37–42.
- Pilkey, O.H., Neal, W.J., Riggs, S.R., and Webb, C.A. 1998. *The North Carolina and its barrier islands – Restless ribbons of sand*, Duke University Press Books.
- Putrevu, U., and Svendsen, I.A. 1999. Three-dimensional dispersion of momentum in wave induced nearshore currents, *Eur. J. Mech. B/Fluids*, 18, 409–427.
- Rogowski, P., Terrill, E., and Chen. J.-L. 2014. Observations of the Frontal Region of a Buoyant River Plume using an Autonomous Underwater Vehicle, *J. Geophys. Res.*, in revision.
- Shi, F., Svendsen, I.A., Kirby, J.T., and Smith, J. M. 2003. A curvilinear version of a Quasi-3D nearshore circulation model, *Coastal Eng.*, 49 (1-2), 99-124.

- Shi, F., Kirby, J. T., Hsu, T.-J., Chen J.-L., and Mieras, R. 2013. *NearCoM-TVD, documentation and users' manual, Research Report, CACR-13-06*, University of Delaware, Newark, Delaware.
- Smith, J. M., Bermudez, H. E., and Ebersole, B. A. 2000. Modeling waves at Willapa Bay, Washington, *Proc 27th Int. Conf. Coastal Engineering*, ASCE, 826-839.
- Soulsby, R.L., Hamm L., Klopman G., Myrhaug D, Simons R.R., and Thomas G.P. 1993. Wave-Current Interaction within and outside the bottom boundary layer, *Coastal Eng.*, 21. pp.41-69.
- Soulsby, R.L. 1997. *Dynamics of marine sands*, Thomas Telford, London.
- Swart, D.H. 1974. *Offshore sediment transport and equilibrium profiles*, Delft Hydraulic Laboratory, Publication no. 131, 217 pp.
- Svendsen, I. A., Haas, K., and Zhao, Q. 2004. *Quasi-3D Nearshore Circulation Model SHORECIRC: Version 2.0, Research Report*, Center for Applied Coastal Research, University of Delaware.
- Toro, E. F. 2009. *Riemann solvers and numerical methods for fluid dynamics: a practical introduction*, Third edition, Springer, New York.
- Van Dorn, W.C. 1953. Wind Stress on an Artificial Pond, *Journal of Marine Research*, Volume 12.
- Warner, J. C., Sherwood, C. R., Signell, R. P, Harris, C. K., and Arango, H. G. 2008. Development of a three dimensional, regional, coupled wave, current, and sediment transport model, *Comput. Geosci.*, 34 10 , 1284 - 1306.
- Wargula, A., Raubenheimer, B., Elgar, S. 2014. Wave-driven along-channel subtidal flows in a well-mixed ocean inlet, *J. Geophys. Res.*, 119 5 , 2987-3001.(b).
- Willmott, C. J. 1981. On the validation of models, *Phys. Geogr.*, 2, 184-194.
- Wolf, J., Prandle, D. 1999. Some observations of wave-current interaction, *Coastal Eng.*, 371, 471-485.